JOURNAL OF PROPULSION AND POWER
Vol. 12, No. 3, May–June 1996

# Influence of Formation Processes on Oblique Detonation Wave Stabilization

K. Ghorbanian* and J. D. Sterling†
*Advanced Projects Research, Inc., Santa Rosa, California 95403*

**In this article we report steady, two-dimensional, inviscid solutions for the near field and far field of a supersonic reactive flow over a variable-double-ramp geometry. The incident shock wave compresses and heats the reactants that will combust after flowing some induction length. Upon reaction, a detonation wave forms and intersects the leading wave at some distance from the ramp surface. In this article, reaction-polar diagrams are developed and the detonation branch solutions are used to investigate the wave interaction processes that may lead to a steady three-wave structure. By considering this formation process new oblique detonation wave stabilization criteria based on the freestream conditions and ramp geometry are provided.**

## Introduction

THE idea of harnessing a stabilized detonation wave for propelling hypersonic air-breathing vehicles and hypervelocity projectile launchers is an old one and is still under investigation. Since only the normal component of the velocity leaving an oblique detonation wave (ODW) is subsonic or sonic, supersonic flow can be maintained throughout the combustor. Assuming that an ODW can be stabilized, an ODW engine will require less inlet diffusion than a diffusive-burning supersonic combustion ramjet (scramjet) engine. An ODW engine design requires premixing of the fuel and air while avoiding ignition upstream of the stabilizing wedge/cowl.[1] Although scramjet engines do not suffer this constraint, premixing has been shown to offer significant benefits to scramjet cycle performance.[2] Furthermore, a recent finite rate chemistry analysis suggests that premixing may be necessary for scramjet combustion in the range of flight Mach numbers of 8–16, because of excessively long mixing and chemical induction times.[3] It should be emphasized that scramjet engine designs with any significant degree of premixing may lead to an undesirable ODW formation.

It is important to distinguish between shock-induced combustion processes and pressure-coupled shock-induced combustion phenomena, i.e., detonation. As is well known, pressure rises because of heat release in a supersonic flow may create compression waves that can steepen into shock waves. Problems associated with combustion-induced compression necessitate the presence of isolators in dual-mode ramjet/scramjet designs.[4] In addition, under some circumstances, thermal occlusion may result in a detonation wave structure. Consequently, detonation phenomena must be considered during any scramjet engine development program.

Although the theory of compression and combustion waves is fairly well developed, there remain misconceptions of cause and effect with regard to the interactions between gasdynamics and chemical processes. Previous attempts to stabilize ODWs in the laboratory have been inconclusive, due in part to limited-approach Mach numbers, but also because of a fundamental lack of understanding of detonation wave mechanics. Early results from shock-tunnel experiments on wedge configurations performed in the 1960s were interpreted as detonation where the term shock-induced combustion would be more appropriate.[2,5,6] Another experimental approach involved the firing of projectiles at different supersonic velocities into a variety of premixed combustible gases.[7–12] Significant insight on detonation structure and the corresponding stability criteria were also obtained in two-layer shock-tube experiments.[13,14] Further historical reviews may be found in Refs. 15 and 16.

The main goal of this investigation is to introduce some key ideas that have to be considered for any hypersonic air-breathing engine design. In this article we report steady, two-dimensional solutions for the near- and far-field regions of a variable double-ramp immersed in a supersonic flow of a homogeneous reactive mixture, as presented in Fig. 1. This double-ramp configuration is relevant to external propulsion and ram accelerator concepts and provides a fundamental geometry for the study of hypersonic reacting flows.[17–22]

In the following section, we begin with a discussion of traditional Rankine–Hugoniot analysis and a review of the resulting reaction polars for combustion waves. Attention is devoted to simplified inviscid system analysis in which various configurations of discontinuous compression, expansion, deflagration, and detonation waves are analyzed to delineate various possible solutions. In contrast to previous analytical ODW stabilization studies, the present analysis zooms-in to consider the finite chemical induction time of the reactants downstream of the leading nonreacting shock wave on the wedge. Reaction-polar solutions for the near field of the double-ramp con-

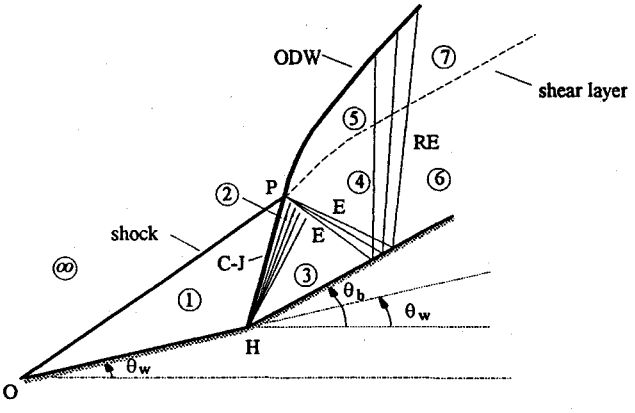


**Fig. 1 Schematic diagram of an unconfined variable double-ramp immersed in a supersonic combustible flow.**

Received May 26, 1995; revision received Sept. 22, 1995; accepted for publication Sept. 23, 1995. 

*Research Scientist; also Visiting Faculty in Aeronautics, California Institute of Technology, Pasadena, CA 91125. Member AIAA.

†Research Scientist; also Lecturer in Jet Propulsion, California Institute of Technology, Pasadena, CA 91125. Member AIAA.

figuration shown in Fig. 1 are developed. The results demonstrate regimes of ODW stabilization that extend the results presented in Ref. 15 by considering the formation processes near the leading edge. In addition, the dependencies of the ODW stabilization criteria on the freestream Mach number and the heat release are presented. Finally, various possible far-field ODW configurations are discussed.

## Rankine–Hugoniot Analysis

### General Features of Reaction Polars

Before delving into multiple-wave interactions of the double-ramp flowfield, it is useful to review the traditional Rankine–Hugoniot analysis, to establish limit cases and nomenclature. The Rankine–Hugoniot relations are particularly useful for investigating, understanding, and classifying systems in which the major changes in the values of the flow variables, as well as the effects of viscosity, diffusion, and thermal conductivity are collapsed into a discontinuity, i.e., compression and combustion waves. A clear presentation of standing ODWs based on the Rankine–Hugoniot analysis is provided in Ref. 15. Further, a number of analytical and numerical studies of stabilized ODWs are reported in which the results are compared with the analysis presented in this reference. In this section, we offer more insight on the subject matter by presenting the general features of reaction polars.

Figure 2 depicts the supersonic flow of an ideal gas through an oblique discontinuity that is inclined at an angle $\beta$ from the incoming flow direction. The flow is turned through a deflection angle $\theta$. For both adiabatic and diabatic flows, the conservation laws of mass, normal momentum, tangential momentum, and energy yield

$$\rho_\infty u_{\infty n} = \hat{\rho}\hat{u}_n \tag{1}$$

$$p_\infty + \rho_\infty u_{\infty n}^2 = \hat{p} + \hat{\rho}\hat{u}_n^2 \tag{2}$$

$$(\rho_\infty u_{\infty n})u_{\infty t} = (\hat{\rho}\hat{u}_n)\hat{u}_t, \quad \text{or} \quad u_{\infty t} = \hat{u}_t \tag{3}$$

$$h_\infty + (u_{\infty n}^2/2) = \hat{h} + (\hat{u}_n^2/2) \quad (\text{since} \quad u_{\infty t}^2 = \hat{u}_t^2) \tag{4}$$

where the symbols $\infty$ and $\wedge$ denote upstream and downstream conditions, respectively. To complete the system of the equations, the ideal gas equation of state is assumed to apply

$$p = \rho RT \tag{5}$$

With the assumption of heat released implicitly because of chemical reaction, Eq. (4) may be used as is, provided the enthalpies $h_\infty$ and $\hat{h}$ include both the chemical enthalpy of formation and the sensible enthalpy. Accurate results at high temperature and pressure require the use of variable specific heats and complex chemical equilibrium and kinetics calculations.[23] For purposes of exposition, it is assumed that $Q_\infty$ units of heat per unit mass are added to the fluid to represent the sensible heat release because of combustion. Further, assuming that the fluid has a constant specific heat capacity and does not change composition by heat addition, Eq. (4) may be rewritten as

$$c_pT_\infty + (u_{\infty n}^2/2) + Q_\infty = c_p\hat{T} + (\hat{u}_n^2/2) \tag{6}$$

Notice that the previous set of equations hold for combustion waves in general, that is, deflagration as well as detonation. The combination of the conservation equations, the equation of state, and the kinematic relations of the geometry from Fig. 2 result in a density ratio expressed by

$$\frac{\rho_\infty}{\hat{\rho}} = \frac{\hat{u}_n}{u_{\infty n}} = \frac{\tan(\beta - \theta)}{\tan\beta} \tag{7}$$

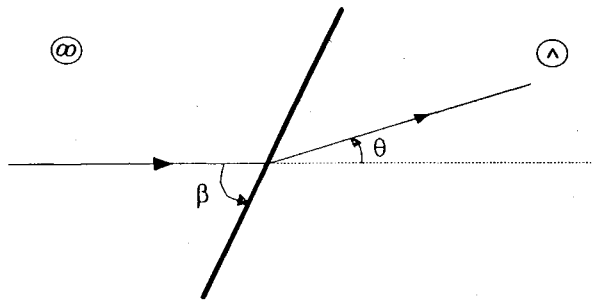


**Fig. 2 Plane oblique discontinuity geometry.**

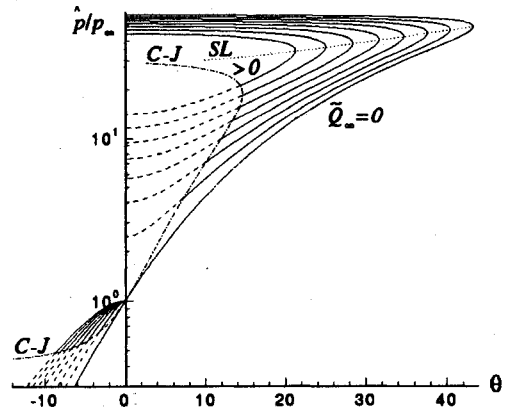


**Fig. 3 Generalized reaction polars ($M_\infty = 7.0$).**

which after some algebraic manipulations may be rewritten as

$$\frac{\rho_\infty}{\hat{\rho}} = \frac{1 + \gamma M_{\infty n}^2}{(\gamma + 1)M_{\infty n}^2} \pm \frac{\sqrt{(1 - M_{\infty n}^2)^2 - 2(\gamma + 1)M_{\infty n}^2\tilde{Q}_\infty}}{(\gamma + 1)M_{\infty n}^2} \tag{8}$$

where $\tilde{Q}_\infty$ is the second Damköhler parameter defined as

$$\tilde{Q}_\infty = Q_\infty/c_pT_\infty \tag{9}$$

Furthermore, the Mach number is defined as

$$M_\infty \equiv u_\infty/\sqrt{\gamma RT_\infty} \tag{10}$$

where $M_{\infty n} \equiv M_\infty \sin\beta$, and $\gamma = c_p/c_v$ is the ratio of constant specific heats. Finally, substituting Eq. (8) into the normal momentum equation and rearranging gives

$$\hat{p}/p_\infty = 1 + \gamma M_{\infty n}^2[1 - (\rho_\infty/\hat{\rho})] \tag{11}$$

In the analysis of steady two-dimensional flow, a useful set of results for computing wave interactions is obtained by plotting the pressure ratio $\hat{p}/p_\infty$ vs the turning angle $\theta$ for various $\tilde{Q}_\infty$. These curves are presented in Fig. 3 and will be referred to as reaction polars. It is apparent from inspection of Fig. 3 that the reaction polars are divided into two nonoverlapping branches: an upper branch for which the pressure ratio $\hat{p}/p_\infty > 1$, called detonation polars, and a lower branch for which the pressure $\hat{p}/p_\infty < 1$, called deflagration polars. By definition, the detonation (deflagration) polars represent flows with a normal component of the freestream Mach number $M_{\infty n}$ that is supersonic (subsonic).

We first consider the general characteristics of detonation polars. As illustrated in Fig. 3, for adiabatic flows, for a given deflection angle $\theta$ there are either two solutions to the oblique shock relations, or none at all. In addition, the detonation polar solutions may be divided by the sonic line *SL* and termed weak solutions corresponding to downstream supersonic flow and strong solutions corresponding to downstream subsonic flow.

Further examination of Fig. 3 indicates that an additional classification for diabatic flows is necessary. This classification is based on whether the normal component of the downstream Mach number $\hat{M}_n$ is subsonic, sonic, or supersonic. For diabatic flows, states with $\hat{M}_n = 1$, corresponding to Chapman–Jouguet (C–J) detonation waves, are represented by the C–J curve. Points on the constant $\tilde{Q}_\infty$ dashed lines to the left of the C–J point are underdriven waves with $\hat{M}_n > 1$. Points on the constant $\tilde{Q}_\infty$ solid lines to the right of the C–J point have $\hat{M}_n < 1$ and are overdriven. To be consistent with the terms weak and strong as applied to adiabatic oblique shock waves, points within the C–J curve and below the sonic line will be referred to as weak overdriven, and above the sonic line as strong overdriven. However, since all strong oblique shock waves are overdriven, they will be called simply strong ODWs. It is also apparent from inspection that there is a maximum turning angle $\theta_{max}$ beyond which an oblique detonation wave will detach or unstart, just as in the case of oblique shock waves without heat addition, but with a reduced range of turning angles with increasing amounts of heat release. In this article, we will demonstrate that detonation stabilization on a ramp is limited by additional detachment criteria.

#### Significance of the C–J Condition

As noted earlier, there are three distinct classes of ODWs that must be considered in detonation wave stability analyses for applications to propulsive devices. The boundary between underdriven ODWs and weak overdriven ODWs is delimited by the C–J state, which is the point of minimum wave angle $\beta$ on each locus of states for diabatic flows.[15,24] Since total pressure loss increases both with the amount of heat release $\tilde{Q}$ and wave angle $\beta$, the C–J turning angle $\theta_{cj}$ corresponds to the minimum total pressure loss for the given approach condition. Consequently, the C–J state provides a limiting condition for ODW engine design.

Having established the significance of the C–J state as a bound, Rankine–Hugoniot relations at the C–J point provide the most convenient forms for the analysis of ODWs. The maximum possible heat addition satisfying the conservation equations for a given value of approach Mach number $M_\infty$ is defined as the C–J heat addition $\tilde{Q}_{cj}$, which is given by

$$\tilde{Q}_{cj} \equiv \frac{(1 - M_\infty^2)^2}{2(\gamma + 1)M_\infty^2} \tag{12}$$

By definition, the C–J wave angle $\beta_{cj}$ is

$$\beta_{cj} \equiv \sin^{-1}(M_{cj}/M_\infty) \tag{13}$$

where $M_{cj}$ is given by

$$M_{cj} \equiv \sqrt{[1 + \tilde{Q}_\infty(\gamma + 1)] \pm \sqrt{[1 + \tilde{Q}_\infty(\gamma + 1)]^2 - 1}} \tag{14}$$

$M_{cj}^{(+)}$ and $M_{cj}^{(-)}$ correspond to the C–J Mach numbers of normal detonation and deflagration waves, respectively, in which heat $\tilde{Q}_\infty$ is released. Further, the C–J density and pressure ratios can be shown to be

$$\left(\frac{\rho_\infty}{\hat{\rho}}\right)_{cj} \equiv \frac{1 + \gamma M_{cj}^2}{(\gamma + 1)M_{cj}^2} \tag{15}$$

$$\left(\frac{\hat{p}}{p_\infty}\right)_{cj} \equiv \frac{1 + \gamma M_{cj}^2}{\gamma + 1} \tag{16}$$

Finally, making use of Eq. (7) with the trigonometric identity

$$\tan(\sin^{-1}x) = x/\sqrt{(1 - x)} \tag{17}$$

the C–J turning angle $\theta_{cj}$ is given by

$$\theta_{cj} \equiv \beta_{cj} - \tan^{-1}\left[\frac{1 + \gamma M_{cj}^2}{(\gamma + 1)M_{cj}^2\sqrt{(M_\infty/M_{cj})^2 - 1}}\right] \tag{18}$$

The different regions of reaction polars presented in this section are not all physically accessible and their physical occurrence is sensitive to the particular geometrical configuration and freestream conditions. On the basis of numerical calculations and experimental measurements, the usual detonation structure may be represented by a shock wave followed by a pressure-coupled deflagration front, that is, the Zeldovich–von Neumann–Döring (ZND) model.[25] The normal component of the velocity downstream of the nonreacting shock wave is subsonic. As is well known, it is not possible to have heat addition to a subsonic flow and proceed past the sonic condition. Therefore, the first restriction on the reaction polars presented earlier is that the underdriven detonation branch is not accessible. For the same reason, the strong deflagration branch is not physically accessible.

## Analysis of a Fundamental System

In this section we will identify the fundamental two-dimensional steady solutions that can exist in a supersonic flow of a combustible gas well in excess of the C–J speed over the variable-double-ramp configuration illustrated in Fig. 1. The relevant geometrical parameters presented in this figure are, the forward ramp half-angle $\theta_w$, the base angle $\theta_b$, the wedge surface $\overline{OH}$, and the base surface $\overline{HB}$. As the reactant gas passes point $O$, a nonreacting oblique shock wave is generated. This shock wave compresses and heats the reactants that will combust after flowing an induction length $l_{ind}$. In the present study, systems of reactant composition, freestream properties, and wedge angles will be considered, which make this induction length $l_{ind}$ exactly equal to the distance $\overline{OH}$. Thus, we may define the flow to have a first Damköhler number $Da = t_{fluid}/t_{chem} = 1$. In other words, we zoom-in to observe the separation region between the nonreacting shock wave and the heat release front. In this region, the reactant static pressure and temperature are sufficiently high to induce radical formation reactions. However, the product formation and the related energy release are not significant since the radical concentration is not yet able to sustain continuous product formation. Passing through this induction region, the radical accumulation will reach a level capable of supporting a continuous energy release.

It is evident that different flowfield configurations may be obtained depending on the magnitude of the base angle $\theta_b$. We begin with a discussion of possible configurations by considering small enough base angles that a deflagration wave is formed parallel to the leading nonreacting shock. Acceleration of the subsonic normal velocity component flowing into the deflagration wave is demanded by the conservation law of mass, while the tangential velocity component remains constant. Therefore, a streamline through such an oblique deflagration wave is deflected towards the direction of the normal to the deflagration surface. Thus, the flow is turned and accelerated through the deflagration front by the negative flow deflection angle $-\delta$, as seen in Fig. 4a. It is apparent from inspection of this figure that if $\alpha$, the angle enclosed by the forward ramp and the base ramp, is smaller than $(\pi - \delta)$, the flow has to be brought parallel to the base surface $\overline{HB}$, that is, the fluid must be further accelerated by a centered Prandtl–Meyer expansion emanating from point $H$. There is a minimum angle $\alpha_{min}$ corresponding to the maximum Prandtl–Meyer angle $\nu_{max}$, below which the flow can no longer be kept parallel to the base surface $\overline{HB}$ as shown in Fig. 4a.

An increase of $\alpha$ above $\alpha_{min}$ causes the intensity of the Prandtl–Meyer expansion angle $\nu$ to decrease while the strength and location of both the leading nonreacting shock

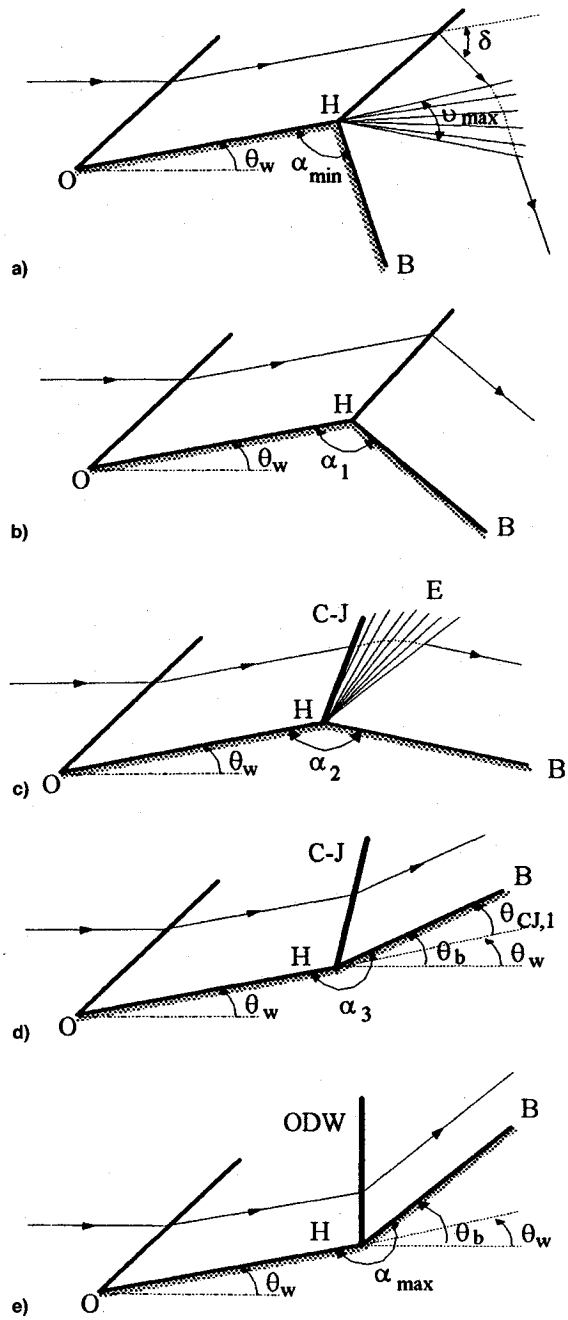


**Fig. 4 Potential flow configurations for an unconfined variable double-ramp.**

wave as well as the deflagration front remain unaffected. At some base ramp position $\alpha_1$, the expansion fan will vanish and the flow immediately behind the deflagration front will be parallel to the base surface as shown in Fig. 4b, that is, $\alpha$ is exactly equal to $(\pi - \delta)$.

With a further infinitesimal increase of $\alpha$, the flow immediately behind the deflagration wave would be deflected towards the base surface $\overline{HB}$. However, since the flow must remain parallel to the surface, the pressure increases, resulting in the generation of compression waves that steepen to form a C–J detonation wave. Additionally, a centered Prandtl–Meyer expansion must immediately follow the C–J detonation to return the flow to be parallel to the base surface (shown in Fig. 4c).

As an explanation of the C–J detonation formation, we introduce a one-dimensional unsteady analogy of the two-dimensional steady flow. This one-dimensional unsteady analogy is represented by a twice-accelerated piston at the end of a

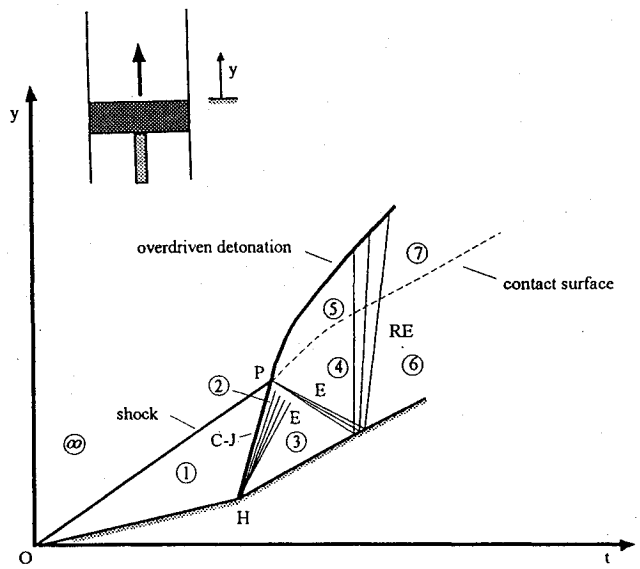


**Fig. 5 Unsteady shock-tube geometry.**

tube filled with reactive gases. An impulsive start generates a shock wave that heats the gas at the piston face, which subsequently begins to react just as the piston velocity is impulsively changed again. A transition from deflagration to detonation (DDT) results and an unsteady expansion enforces the piston velocity on the gas between the detonation and the piston. The time-location or $t$–$y$ diagram of the one-dimensional unsteady flow, shown in Fig. 5, has the same character as the steady flow of Fig. 4c. In this analogy, it is clear that the DDT should occur rapidly after the initial heat release at the piston face. The reason is that the radical concentrations have been increased and as compression waves propagate away from the piston, the reactants respond immediately and a C–J wave results. In addition, the detonation cell size of this C–J wave will be orders of magnitude smaller than any characteristic dimension of the representative geometry. The analogous two-dimensional steady flow will have a planar C–J detonation.[26]

Returning now to the two-dimensional steady flow analysis, we observe in Figs. 4c and 4d, that by increasing the enclosed angle $\alpha$, the intensity of the expansion fan decreases. At some base ramp position $\alpha_3$, which is uniquely determined by the reactant composition, freestream condition, and the forward ramp half-angle, the expansion fan will vanish and the flow immediately behind the C–J detonation wave will be parallel to the base surface $\overline{HB}$, that is, $\theta_b = \theta_{b,cj} \equiv \theta_w + \theta_{cj,1}$. The subscript 1 denotes the induction region between the leading nonreacting shock wave and the incoming ODW.

Finally, for a further increase of $\alpha$, the conservation laws require an overdriven ODW to result (Fig. 4e) since more mechanical energy will be converted from the freestream to support the overdriven detonation wave. However, if the enclosed angle becomes sufficiently large, $\alpha > \alpha_{max}$, the converted mechanical energy from the freestream becomes too great and the ODW detaches as in the case of a blunt body immersed in a superdetonative combustible flow.

## Near-Field Three-Wave Structure

### Base Ramp Angles for C–J Detonation

As a starting point, we consider a double-ramp configuration at specified freestream conditions for which no Prandtl–Meyer expansion fan will be generated at point $H$. The leading nonreacting shock wave originating at point $O$ deflects the supersonic flow to an angle $\theta_w$ as illustrated in Fig. 1. By passing through the leading wave, both the C–J Mach number and the second Damköhler parameter downstream of the leading wave will be changed. Thus, for variable $\theta_w$ the amount of heat ad-

dition $\tilde{Q}_1$ released across the C–J detonation wave, emanating at point $H$, will also vary and is given by

$$\tilde{Q}_1 = \tilde{Q}_\infty/(\hat{T}_1/T_\infty) \tag{19}$$

Further, for stabilized detonation waves, the velocity downstream of the leading nonreacting shock wave must exceed the local C–J speed of the reactants, that is, $M_1 > M_{cj,1}$.

In this section, we will focus on the condition for which $\alpha = \alpha_3$, so that the superdetonative flow downstream of the leading wave in Fig. 1 encounters a base ramp whose deflection angle will produce a C–J detonation wave with downstream flow parallel to the base surface $\overline{HB}$ ($\theta_b = \theta_{b,cj}$). This process may be presented as a detonation polar as shown in Fig. 6. The adiabatic jump condition $\infty - 1$ lies on the shock polar *SP*. From this condition, 1, we may draw the detonation polar *DP* for $M_1$ and $\tilde{Q}_1$. The conditions downstream of the C–J detonation are represented by point 2 on the figure. Two detonation polars are presented corresponding to $\theta_w = 10$ and 35 deg.

We now address the dependency of the base ramp angle $\theta_{b,cj}$ with variation of the forward ramp half-angle $\theta_w$ at constant freestream Mach number $M_\infty$ and second Damköhler parameter $\tilde{Q}_\infty$. Starting with $\theta_w = 0$ deg, it is apparent that $\theta_{b,cj}$ equals the C–J deflection angle based on the freestream properties, $M_\infty$ and $\tilde{Q}_\infty$. Now let $\theta_w$ increase. Note that there exists a maximum forward ramp half-angle $\theta_{w,max}$ beyond which the leading nonreacting shock wave becomes detached. Figure 7 shows the variation of the following quantities downstream of the leading nonreacting shock wave with $\theta_w$: the Mach number $M_1$, the C–J Mach number $M_{cj,1}$, and the second Damköhler parameter $\tilde{Q}_1$. As seen in this figure, an attached C–J detonation wave structure initiated at point $H$ will only occur if $\theta_w$ is less than both $\theta_{w,max}$ and $\theta_{w,cj}$ (above which $M_1 < M_{cj,1}$). Consequently, based on stability considerations, the range of the forward ramp half-angle $\theta_w$, within which ODWs may be attached and stabilized, is restricted to the interval

$$0 \le \theta_w \le \theta_{w,cj} \quad \text{where} \quad \theta_{w,cj} < \theta_{w,max} \tag{20}$$

with the corresponding range of the second Damköhler parameter

$$\tilde{Q}_{1(\theta_w=\theta_{w,cj})} \le \tilde{Q}_1 \le \tilde{Q}_{1(\theta_w=0)} \tag{21}$$

Figure 8 illustrates the aforementioned relationship between $\theta_{b,cj}$ and $\theta_w$ at constant $M_\infty$ and $\tilde{Q}_\infty$ on a detonation polar. While curve *SP* presents the shock polar ($\tilde{Q}_\infty = 0$), curve *CS* shows the locus of C–J states as a function of $\theta_w$. The points on curve *SP* labeled 1 represent the adiabatic jump states for corresponding forward ramp half-angles $\theta_w$, whereas points 2 on curve *CS* correspond to base ramp angles $\theta_{b,cj}$. It is also apparent that the $\theta_{b,cj}$ values are bounded by points labeled *i* and *f* corresponding to $\theta_w = 0$ deg and $\theta_w = \theta_{w,cj}$, respectively [Eqs. (20) and (21)].

### Detonation Polar Solutions

It was previously shown that for a fixed forward ramp half-angle $\theta_w$ at constant freestream properties, base ramp angles $\theta_b$ within the limits $\alpha_1 < \alpha < \alpha_3$ will result in a C–J detonation wave followed by a centered Prandtl–Meyer expansion fan emanating at point *H*. Although the normal velocity component downstream of the leading nonreacting shock wave is subsonic, the normal velocity component upstream of the detonation wave is supersonic. As a result, disturbances propagate upstream and the two waves will intersect at point *P* in Fig. 1. These two intersecting discontinuities will be referred to as incoming waves.

As presented in Fig. 1, the flowfield near the shock/C–J detonation intersection contains a transmitted detonation wave

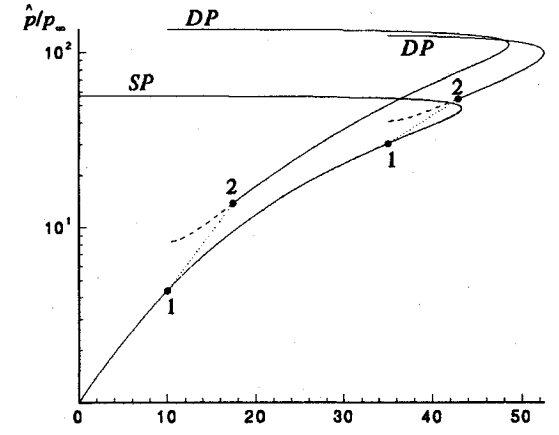


**Fig. 6 Composite shock/detonation polar ($M_\infty$ = 7.0 and $\tilde{Q}_\infty$ = 1.0).**

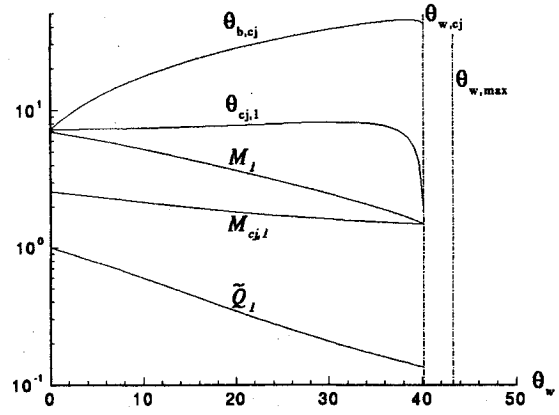


**Fig. 7 Variation of the freestream properties across a nonreacting shock wave ($M_+$ = 7.0 and $\tilde{Q}_\infty$ = 1.0).**

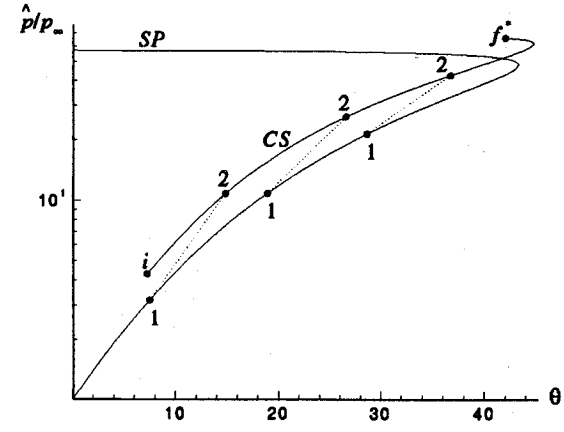


**Fig. 8 Detonation polar for possible C–J states ($M_\infty$ = 7.0 and $\tilde{Q}_\infty$ = 1.0).**

and a Prandtl–Meyer expansion fan emanating from point *P*. These two transmitted waves will be referred to as outgoing waves. Note that because of the temperature rise, the fractional change in the Mach number across the leading nonreacting shock wave is much greater than the fractional change in the velocity. Further, since the sum of the entropy rises because of the leading nonreacting shock wave and that because of the C–J detonation wave is less than that for the outgoing ODW for the same approach condition, a free shear layer or an entropy layer, divides the flow that has passed through the two incoming waves from the flow that has passed through a single outgoing ODW.

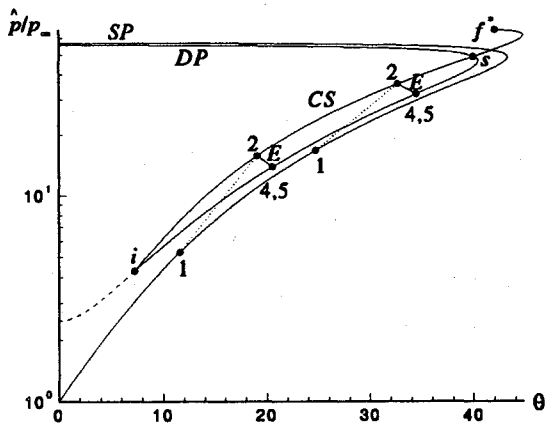


**Fig. 9 Detonation polar for constant freestream properties ($M_\infty$ = 7.0 and $\tilde{Q}_\infty$ = 1.0).**

Having discussed the existence of the shear layer, we now consider the matching of flow direction and pressure across the shear layer. The most convenient manner of visualizing such a solution is by means of detonation polar ($p - \theta$) diagrams. The flow in region 5 is turned through an angle $\theta_5$ from the freestream direction by passing through the outgoing ODW, whereas the flow in region 4 is turned by the same amount from the freestream direction by passing through the leading nonreacting shock wave, the incoming C–J detonation wave, and the expansion fan emanating from point *P*. Furthermore, although the properties such as temperature, density, velocity, etc., are different across the shear layer, the static pressure must remain constant, i.e., $p_5/p_\infty = p_4/p_\infty = (p_1/p_\infty)(p_2/p_1)(p_4/p_2)$. In this section, attention is focused on the neighborhood of point *P* (regions labeled ∞, 1, 2, 4, and 5 in Fig. 1).

The dynamic compatibility requirements discussed previously demand that a single point on a detonation polar diagram represent the flowfield conditions in both regions 4 and 5. Introducing Fig. 9, we note that the conditions of the flow in region 5 lie on curve *DP*. As discussed in the previous section, the conditions in region 2 fall on the curve labeled *CS*. Therefore, the flow conditions in region 2 must be brought to the *DP* curve by gasdynamic means, i.e., shock compression or isentropic expansion. Thus, if a nonreacting shock polar is placed with its origin at point 2, we see that either an isentropic expansion or a shock wave will lead to solutions. In Fig. 9, we consider only the expansion as this is the solution expected in an unconfined flow. These expansion waves are represented by curves labeled *E* in Fig. 9. The intersection points of *E* curves with the *DP* curve represent solutions of the pressure magnitude and flow angle of the outgoing waves. Further, the point labeled *s* is the intersection of curve *CS* with curve *DP*. Thus, the forward ramp half-angle $\theta_{w,s}$ corresponds to the deflection angle for which the downstream state in region 2 is a common state of the detonation polar *DP*, that is, $p_2/p_\infty = p_5/p_\infty$ and $\theta_2 = \theta_5$.

As $\theta_w$ is increased, three distinct classes of solutions may be obtained. The first occurs at a deflection angle within the interval $0 \le \theta_w \le \theta_{w,s}$, for which the flow conditions in region 2 fall within the curve *DP*. As shown previously, in an unconfined geometry, the flow is pressure-matched and parallel in regions 4 and 5 by the presence of a weak overdriven ODW and a centered Prandtl–Meyer expansion fan emanating from point *P*. If $\theta_w$ is exactly equal to $\theta_{w,s}$, the flow may be pressure-matched and parallel by either a strong ODW or by the presence of a weak overdriven ODW and an expansion fan emanating from point *P*. The second class of solutions occurs when $\theta_w$ is increased above $\theta_{w,s}$. The difference between this case and the aforementioned case is that now both possible solutions, the strong ODW and the weak overdriven ODW, are followed by an expansion fan emanating from point *P*.

Finally, a dramatic change occurs when $\theta_w$ is further increased. It is apparent from inspection of Fig. 9 that there is a critical point on curve *CS*, between *s* and *f**, above which curve *E* does not intersect curve *DP* any longer. In other words, if $\theta_w$ is inclined by more than this critical angle $\theta_{w,f}$, relative to the freestream, the total deflection and pressure rise near the base ramp can no longer be matched by any detonative state on curve *DP*. Consequently, the incoming C–J detonation wave originating at point *H* becomes unstable. In this case, the combined effects of flow area occlusion and thermal occlusion from C–J heat release are sufficient to detach the wave structure from point *H*. The resulting wave structure may be stabilized on the forward ramp or may detach from the leading edge entirely.

## Discussion

### Relevance to ODW Stabilization

Our studies indicate that for various values of $\tilde{Q}_\infty$ and $M_\infty$, the range $\theta_{w,s} \le \theta_w \le \theta_{w,f}$ spans only a few degrees. For propulsion applications one is interested in stabilizing weak overdriven ODWs that are not sensitive to flow disturbances. We therefore propose to operate with $\theta_w$ values within the range

$$0 \le \theta_w \le \theta_{w,s} \quad \text{where} \quad \theta_{w,s} < \theta_{w,f} < \theta_{w,\text{CJ}} < \theta_{w,\max} \qquad (22)$$

Further, within this range, the high total pressure losses associated with strong ODWs may also be avoided.

In this study, we have consistently considered the distance $\overline{OH}$ to be exactly equal to the induction length downstream of the leading nonreacting shock wave. It should be noted that this induction length varies with $\theta_w$, $\tilde{Q}_\infty$, and $M_\infty$. For particular freestream conditions, small values of $\theta_w$ may result in excessively long induction lengths $\overline{OH}$. We note that there exist a number of additional detonation initiation sources that may shorten the induction length $\overline{OH}$.[27]

We now address the effect of both $\tilde{Q}_\infty$ and $M_\infty$ on the earlier stability interval [Eq. (22)]. In Fig. 10 detonation polars are plotted for different values of $\tilde{Q}_\infty$ at constant $M_\infty$. In addition, the corresponding *CS* curves are plotted as dashed–dotted lines. By inspection, as $\tilde{Q}_\infty$ increases, the pressure rise because of normal detonation decreases; these conditions correspond to the upper intersections of the *DP* curves with the ordinate. In contrast, for larger $\tilde{Q}_\infty$, the C–J pressure ratio increases; these conditions associated with $\theta_w = 0$ are denoted by the lower plotted solid dots, labeled *i*.

Further, Fig. 10 shows that, the inclination of curve *CS* gets steeper for larger values of $\tilde{Q}_\infty$. Consequently, the intersection point of curve *CS* with its associated detonation polar *DP*, at point *s*, is shifted towards stronger outgoing ODWs with lower subsonic velocities. Recall that at point *s* the flows in regions 4 and 5 are naturally pressure-matched and parallel, but a sec-

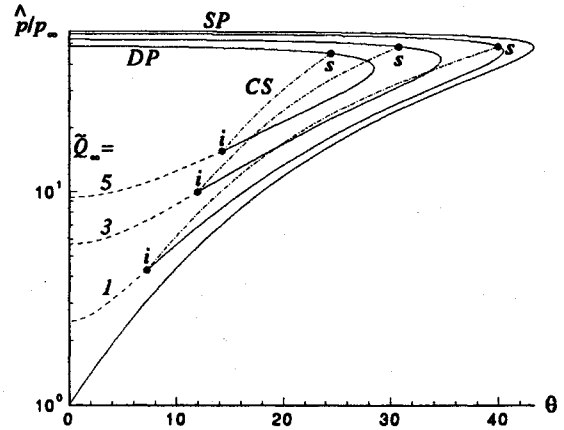


**Fig. 10 Detonation polars for variable heat releases ($M_\infty$ = 7.0).**

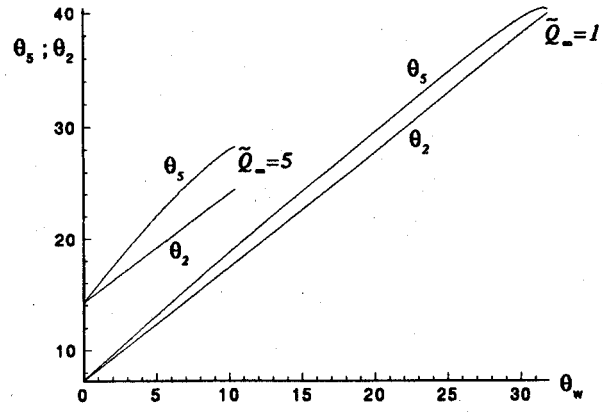


**Fig. 11 Variation of deflection angles with forward ramp half-angle at constant freestream Mach number ($M_\infty$ = 7.0).**

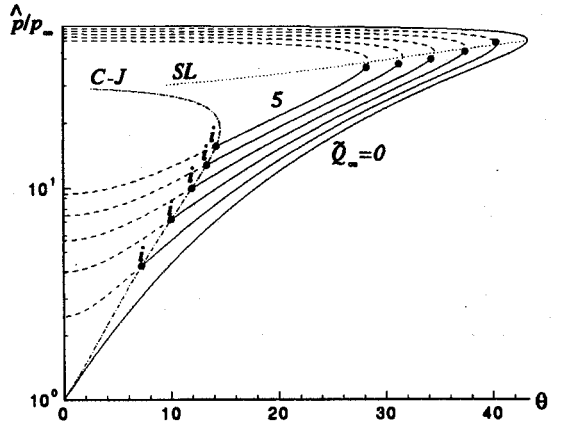


**Fig. 12 Stability plots for constant freestream Mach numbers ($M_\infty$ = 7.0).**

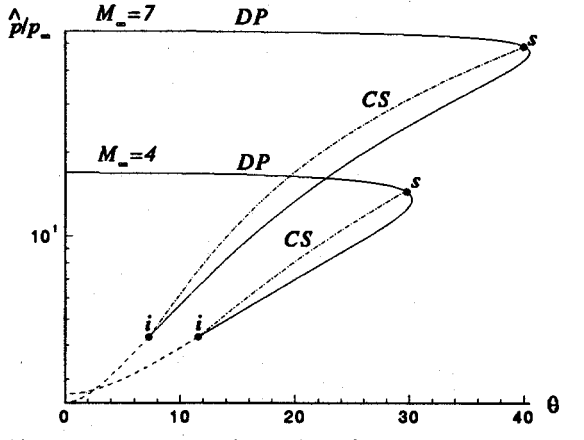


**Fig. 13 Detonation polars for variable freestream Mach numbers ($\tilde{Q}_\infty$ = 1.0).**

ond solution may also occur by the generation of a weak overdriven ODW and a centered Prandtl–Meyer expansion fan between regions 2–4. As is evident from this figure, an increase of $\tilde{Q}_\infty$ will result in an increase of the intensity of the expansion fan at this state.

In Fig. 11, $\theta_5$ and $\theta_2$ are plotted vs $\theta_w$. As already discussed, ODWs are considered to be stabilized for $\theta_w < \theta_{w,s}$. It is apparent from inspection of Fig. 11 that the interval $0 \leq \theta_w \leq \theta_{w,s}$ varies with the value of $\tilde{Q}_\infty$. While for $\tilde{Q}_\infty = 1$ at $M_\infty = 7$, an attached ODW may be stabilized for a forward ramp half-angle within the interval $0 \leq \theta_w \leq 32$ deg, for $\tilde{Q}_\infty = 5$ this interval is reduced to $0 \leq \theta_w \leq 10$ deg. Further, for the same freestream conditions, the operation interval of $\theta_5$ is reduced approximately from $7 \leq \theta_5 \leq 40$ deg to $14 \leq \theta_5 \leq 28$ deg. Additionally, the difference between $\theta_5$ and $\theta_2$ at any $\theta_w$ represents the intensity of the expansion fan emanating from point $P$.

A stability map is developed by using a detonation polar to represent the previous results for various $\tilde{Q}_\infty$, at constant $M_\infty$ in Fig. 12. The solid curves represent regions in which an attached outgoing ODW may be stabilized. The lower end of these curves, points labeled $i$, is a bound that represents $\theta_w$ = 0 conditions (C–J states). The upper end represents solutions for $\theta_w = \theta_{w,s}$ that provide a weak overdriven ODW and a centered Prandtl–Meyer expansion fan between regions 2–4. Points on the dashed constant $\tilde{Q}_\infty$ lines on the lower branch to the left of the C–J point are unphysical underdriven waves. The dashed curves on the upper branch are ruled out by the detachment criteria discussed earlier.

We now investigate the effect of $M_\infty$ on the stability interval presented previously [Eq. (22)]. Figure 13 illustrates detonation polars for different $M_\infty$ at constant $\tilde{Q}_\infty$. As seen in Eqs. (14) and (16) and in Fig. 13, the pressure rises because of normal detonation are very sensitive to $M_\infty$, whereas the C–J pressure ratio, points labeled $i$, remains unaffected. Further, it can be seen from Fig. 13 that, as the inclination of the $CC$ curves gets steeper with larger values of $M_\infty$, the intersection points $s$ occur at higher values of the outgoing deflection angle. As is evident from Fig. 14, the intensity of the centered Prandtl–Meyer expansion fan between regions 2–4 remains almost constant. Further, it is apparent from inspection of Fig. 14 that the stability interval of $\theta_w$ for $\tilde{Q}_\infty = 1$ at $M_\infty = 7$ is reduced to $0 \leq \theta_w \leq 18$ deg for the same $\tilde{Q}_\infty$ at $M_\infty = 4$. The corresponding interval of $\theta_5$ is reduced to $12 \leq \theta_w \leq 30$ deg. Finally, a stability map analogous to that illustrated in Fig. 12

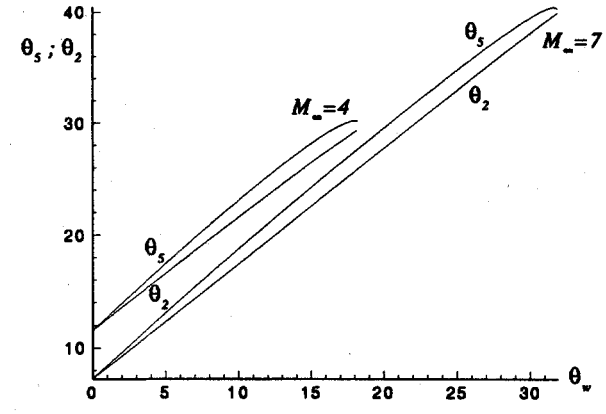


**Fig. 14 Variation of deflection angles with forward ramp half-angle at constant heat release ($\tilde{Q}_\infty$ = 1.0).**

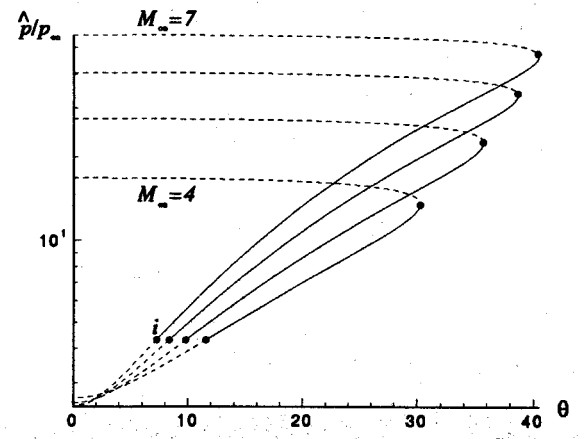


**Fig. 15 Stability plots for constant heat releases ($\tilde{Q}_\infty$ = 1.0).**

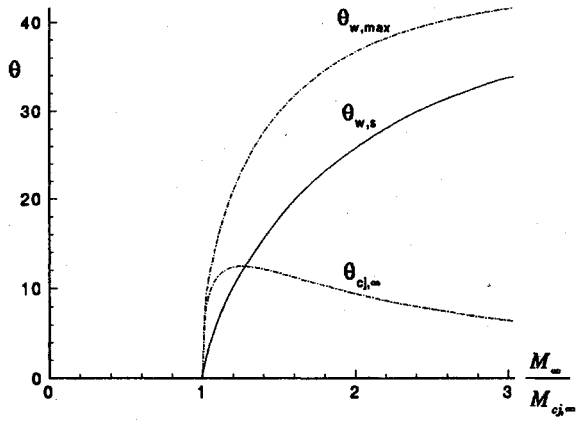


**Fig. 16 Wedge angle range for ODW stabilization at constant heat release ($\tilde{Q}_\infty = 1.0$).**

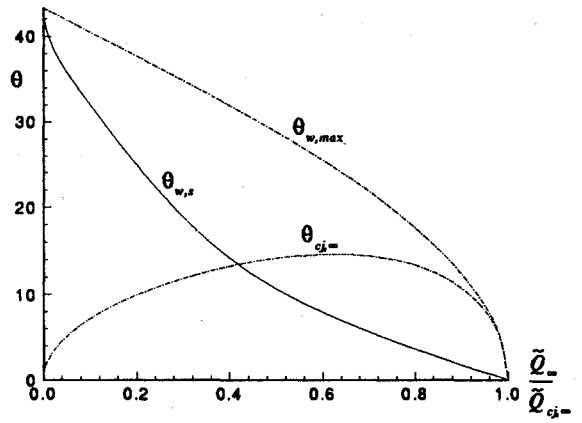


**Fig. 17 Wedge angle range for ODW stabilization at constant freestream Mach number ($M_\infty = 7.0$).**

is shown in Fig. 15. It can be seen by inspection that for a fixed $\tilde{Q}_\infty$ the upper value of the stability interval increases with the freestream Mach number $M_\infty$.

The consequences of these results with regard to propulsion system ODW stabilization are presented in Figs. 16 and 17. By considering the wave formation process, we demonstrated that attached ODWs may be stabilized within the range of wedge angles $0 \leq \theta_w \leq \theta_{w,s}$. In Fig. 16, $\theta_{w,s}$ is plotted as a function of the normalized $M_\infty$ with $M_{cj,\infty}$ at constant $\tilde{Q}_\infty$. For comparison, the range of ODW stabilization proposed in Ref. 15, $\theta_{cj,\infty} < \theta_w < \theta_{w,max}$, is also shown in this figure. There are two primary differences between the results of the present analysis and those of the aforementioned reference. In our theory, the maximum wedge angle at which ODWs may be stabilized has been lowered from $\theta_{w,max}$ to $\theta_{w,s}$, whereas the minimum has been lowered from $\theta_{cj,\infty}$ to zero. The result is that for $M_\infty/M_{cj,\infty}$ less than about 1.3 there is no overlap of ODW stabilization ranges of the two theories.

With regard to the maximum stabilization angle our results are consistent with unsteady numerical simulations reported in Ref. 28. For wedge angles about 10 deg lower than the predicted value of $\theta_{w,max}$, their simulations initially show subsonic flow just downstream of the outgoing ODW. This ODW subsequently moves forward and detaches as described by the present wave-interaction analysis. A similar process can also be seen in the numerical simulations reported in Ref. 29.

In Fig. 17, $\theta_{w,s}$, $\theta_{cj,\infty}$, and $\theta_{w,max}$ are plotted as a function of $\tilde{Q}_\infty$ normalized by $\tilde{Q}_{cj,\infty}$ at constant $M_\infty$. The results are analogous to those discussed in the previous paragraph. While in Fig. 16 ODW stabilization is limited by the C–J Mach number, in Fig. 17 the C–J heat addition limits the operation range. Additionally, for values of $\tilde{Q}_\infty/\tilde{Q}_{cj,\infty}$ greater than about 0.4, there is again no overlap of ODW stabilization ranges of the two theories. In both Figs. 16 and 17 the C–J point represents normal detonation wave for the specified freestream condition.

### Extension of the Results to the Far Field

To this point, solutions have been discussed only for the near-field region of an unconfined double-ramp immersed in a supersonic reactive flow. In this section attention is devoted to the region where wave interactions have ceased, as shown in Fig. 1. In other words, we consider the requirement that the flow far downstream of the outgoing ODW be parallel to the base ramp. We refer to the region where this condition is satisfied as the far field.

The results presented for the near-field wave interactions, for all values of $\alpha > \alpha_1$, consistently show either an overdriven ODW between regions $\infty$ and 5 or a detachment of the wave structure from the double ramp. In either case the overdriven detonation turns the flow away from the angle of the base wall $\overline{HB}$. Thus, some expansion must occur for the flow to be returned to the wall support in the far field, which is shown in regions 6 and 7 in Fig. 1. Note that although the figure shows noninteracting expansion fans, there are actually some reflections from the base wall, shear layer, and the outer ODW. Nonetheless, at some downstream location, the flow behind the detonation will be parallel to the base wall.

Referring again to Fig. 1, recall that for any base angle providing $\alpha > \alpha_1$, a C–J detonation wave will form and will be followed immediately by an expansion fan. This expansion will intersect the overdriven ODW and will weaken it so that the downstream flow will be parallel to the wall. Depending on the base ramp angle, one of the following three far-field solutions is possible.

The first possibility occurs for base ramp angles $\theta_b > \theta_{cj,\infty}$. For these conditions, the expansion will cause the ODW to curve to a shallower angle so that the overdriven ODW weakens, but still remains overdriven with the downstream flow parallel to the base wall. However, if the $\theta_b < \theta_{cj,\infty}$, two far-field solutions may occur. For these conditions, the expansion will weaken the overdriven ODW until it becomes either a C–J wave or until the compression becomes too weak to support a coupled reaction front. In Ref. 30 it was shown that if a C–J detonation wave has been stabilized, $\theta_b$ may be negative. Should a bifurcation of the reaction zone from the shock wave occur, it will happen near the point at which the ODW angle is the C–J wave angle.[12,27,31]

The conclusion that an overdriven outgoing ODW is weakened to provide flow parallel to the base ramp is also supported by schlieren photographs of the three-wave structure in shock-tube experiments.[13,32] Although strong ODWs were often observed in these confined-flow experiments, pressure measurements indicate that the pressure rise of the flow passing near the wall is indeed much higher than the rise through the outgoing ODW. This overpressure along the wedge surface is responsible for the stabilization of the three-wave structure.

## Conclusions

An investigation of steady, two-dimensional, inviscid solutions for the near field and far field of a supersonic reactive flow over a variable-double-ramp geometry has been presented. Reaction-polar diagrams have been used to investigate the wave interaction processes that lead to a steady three-wave structure. The principal assumption of our study was that the length of the forward ramp was exactly equal to the induction length of the reactants upon passing through the leading nonreacting shock wave. Further, the freestream conditions, the amount of the heat release, and the ramp angles are assumed known and are treated as parameters.

Note that in a real combustor environment the aforementioned parameters may be coupled to one another. Indeed, since chemical reaction rates are exponentially dependent on the temperature, the amount and the location of the heat release

is very sensitive to the particular geometry. However, by specifying the induction length exactly equal to the length of the forward ramp, this article introduces a simple analytic system that identifies basic dominant features of hypersonic combusting flows.

The results of the study demonstrate that as the freestream Mach number increases and/or the amount of the heat release decreases, the range of wedge angles over which an ODW may be stabilized increases. The maximum wedge angle for a stabilized ODW occurs when the intersection of the incoming waves results in a strong emanating detonation wave. Since the strong detonation wave yields a subsonic downstream flow, information can propagate upstream and may lead to oscillation or detachment of the wave structure. On the other hand, there is no minimum wedge angle for the establishment of an ODW. It is true that for small wedge angles the induction length may become very large. Nonetheless, radical formation reactions will begin at the wedge surface and will be followed by a process analogous to DDT. By taking the nature of this near-field structure into account, new oblique detonation wave stabilization regimes are presented.

The simplified analysis presented in this article should prove useful for the preliminary design of hypersonic airbreathing propulsion engines. Although the analysis focuses on flame holding in ODW-type engines, it is also applicable to ram accelerator unstart and avoidance of undesirable ODW formation in shock-induced combustion scramjet engines.

## Acknowledgments

We would like to express our gratitude to David T. Pratt for many illuminating discussions on detonation phenomena and to Joseph E. Shepherd for helpful comments.

## References

[1]Dunlap, R., Brehm, R. L., and Nicholls, J. A., "A Preliminary Study of the Application of Steady-State Detonative Combustion to a Reaction Engine," *Jet Propulsion*, Vol. 28, No. 7, 1958, pp. 451–456.

[2]Rubins, P. M., and Bauer, R. C., "A Hypersonic Ramjet Analysis with Premixed Fuel Combustion," AIAA Paper 66-648, June 1966.

[3]Jachimowski, C. J., "An Analytical Study of the Hydrogen-Air Reaction Mechanism with Application to Scramjet Combustion," NASA TP-2791, Feb. 1988.

[4]Heiser, W. H., and Pratt, D. T., *Hypersonic Airbreathing Propulsion*, AIAA Education Series, AIAA, Washington, DC, 1994.

[5]Gross, R. A., and Chinitz, W., "A Study of Supersonic Combustion," *Journal of the Aerospace Sciences*, Vol. 27, No. 7, 1960, pp. 517–524.

[6]Rubins, P. M., and Bauer, R. C., "Review of Shock-Induced Supersonic Combustion Research and Hypersonic Applications," *Journal of Propulsion and Power*, Vol. 10, No. 5, 1994, pp. 593–601.

[7]Chernyi, G. G., "Problems of Hydrodynamics and Continuum Mechanics," *Supersonic Flow Past Bodies with Formation of Detonation and Combustion Fronts*, Society for Industrial and Applied Mathematics, Philadelphia, PA, 1969, pp. 145–169.

[8]Ruegg, F. W., and Dorsey, W. W., "A Missile Technique for the Study of Detonation Waves," *Journal of Research of the National Bureau of Standards*, Vol. 66C, No. 1, 1962, pp. 51–58.

[9]Behrens, H., Struth, W., and Wecken, F., "Studies of Hypervelocity Firings into Mixtures of Hydrogen with Air or with Oxygen," *10th Symposium (International) on Combustion*, The Combustion Inst., Pittsburgh, PA, 1965, pp. 245–252.

[10]McVey, J. B., and Toong, T. Y., "Mechanism of Instabilities of Exothermic Hypersonic Blunt-Body Flows," *Combustion Science and Technology*, Vol. 3, No. 2, 1971, pp. 63–76.

[11]Alpert, R. L., and Toong, T. Y., "Periodicity in Exothermic Hypersonic Flows About Blunt Projectiles," *Astronautica Acta*, Vol. 17, Nos. 4 and 5, 1972, pp. 539–560.

[12]Lehr, H. F., "Experiments on Shock-Induced Combustion," *Astronautica Acta*, Vol. 17, Nos. 4 and 5, 1972, pp. 589–597.

[13]Dabora, E. K., Desbordes, D., Guerraud, C., and Wagner, H. G., "Oblique Detonations at Hypersonic Velocities," *Dynamics of Detonations and Explosions: Detonations*, Vol. 133, Progress in Astronautics and Aeronautics, AIAA, Washington, DC, 1991, pp. 187–204.

[14]Liu, J. C., Liou, J. J., Sichel, M., Kaufmann, C. W., and Nicholls, J. A., "Diffraction and Transmission of a Detonation into a Bounding Explosive Layer," *21st Symposium (International) on Combustion*, The Combustion Inst., Pittsburgh, PA, 1987, pp. 1639–1647.

[15]Pratt, D. T., Humphrey, J. W., and Glenn, D. E., "Morphology of Standing Oblique Detonation Waves," *Journal of Propulsion and Power*, Vol. 7, No. 5, 1991, pp. 837–845.

[16]Shepherd, J. E., "Detonation Waves and Propulsion," *Combustion in High-Speed Flows*, 1994, pp. 373–420.

[17]Yungster, S., and Rabinowitz, M. J., "Computation of Shock-Induced Combustion Using a Detailed Methane-Air Mechanism," *Journal of Propulsion and Power*, Vol. 10, No. 5, 1994, pp. 609–617.

[18]Rom, J., and Avital, G., "The External Propulsion Accelerator: Scramjet Thrust Without Interaction with Accelerator Barrel," AIAA Paper 92-3717, June 1992.

[19]Grismer, M. J., and Powers, J. M., "Calculations for Steady Propagations of a Generic Ram Accelerator Configuration," *Journal of Propulsion and Power*, Vol. 11, No. 1, 1995, pp. 105–111.

[20]Chinitz, W., Bakos, R. J., and Erdos, J. I., "Experimental Requirements for the Study of Shock-Induced Premixed Combustion," AIAA Paper 94-3099, June 1994.

[20]Figueira da Silva, L. F., Deshaies, B., and Champion, M., "A Numerical Study of Ignition Within Hydrogen-Air Supersonic Boundary Layers," *AIAA Journal*, Vol. 31, No. 5, 1993, pp. 884–890.

[22]Hertzberg, A., Bruckner, A. P., and Bogdanoff, D. W., "Ram Accelerator: A New Chemical Method for Accelerating Projectiles to Ultrahigh Velocities," *AIAA Journal*, Vol. 26, No. 2, 1988, pp. 195–203.

[23]Pratt, D. T., "Calculation of Chemically Reacting Flows with Complex Chemistry," *Studies in Convection*, edited by B. E. Launder, Vol. II, Academic, New York, 1977.

[24]Ghorbanian, K., "Superdetonative Flow of Gaseous Propellant Mixtures over Sphere-Cone Bodies," Ph.D. Dissertation, Univ. of Washington, Seattle, WA, March 1993.

[25]Williams, F. A., *Combustion Theory*, Addison–Wesley, Reading, MA, 1988.

[26]Ghorbanian, K., and Sterling, J. D., "Detonation Initiation on a Wedge in a Supersonic Reacting Flow," AIAA Paper 95-2563, July 1995.

[27]Ghorbanian, K., and Pratt, D. T., "An Estimate of the Doomed Propellant Fraction for a Superdetonative Ram Accelerator," AIAA Paper 93-0359, Jan. 1993.

[28]Li, C., Kailasanath, K., and Oran, E. S., "Detonation Structures Behind Oblique Shocks," *Physics of Fluids*, Vol. 6, April 1994, pp. 1600–1611.

[29]Lefebvre, M. H., and Fujiwara, T., "Numerical Modeling of Combustion Processes Induced by a Supersonic Conical Blunt Body," *Combustion and Flame*, No. 100, 1995, pp. 85–93.

[30]Ashford, S. A., and Emanuel, G., "Wave Angle for Oblique Detonation Waves," *Shock Waves*, Vol. 4, No. 3, 1994, pp. 327–329.

[31]Chernyi, G. G., Self-Similar Problems in the Flow of Combustible Mixtures of Gases Past Bodies, *Izv. Akad. Nauk. SSSR Mehkanika Zhidkosti i Gaza*, No. 6, 1966, pp. 10–24.

[32]Desbordes, D., Hamada, L., and Guerraud, C., "Supersonic H2-Air Combustions Behind Oblique Shock Waves," *Shock Waves*, Vol. 4, No. 6, 1995, pp. 339–345.